International Journal of Solids and Structures 46 (2009) 2514–2526

Contents lists available at ScienceDirect

International Journal of Solids and Structures

journal homepage: www.elsevier.com/locate/ijsolstr

Implicit boundary method for determination of effective properties of composite microstructures

Ravi K. Burla, Ashok V. Kumar *, Bhavani V. Sankar

Department of Mechanical and Aerospace Engineering, University of Florida, 106 MAE-C, P.O. Box 116300, Gainesville, FL 32611-6300, USA

ARTICLE INFO

Article history:
Received 22 February 2008
Received in revised form 23 December 2008
Available online 20 February 2009

Keywords:
Fiber composites
Implicit boundary method
Micromechanical analysis
Structured grid analysis
Extended finite element method (X-FEM)

ABSTRACT

A method that uses a structured grid to perform micromechanical analysis for determining effective properties of a composite microstructure is presented. This approach eliminates the need for constructing a mesh that has nodes along the interfaces between constituent materials of the composite. Implicit boundary method is used to ensure that interface conditions are satisfied at the material boundaries. In this method, solution structures for test and trial functions are constructed using approximate step functions such that the interface conditions are satisfied, even if there are no nodes on the material interface boundary. Since a structured grid does not conform to the geometry of the analysis domain, the geometry of the microstructure is defined independently using equations of the interface boundary curves/surfaces. Structured grids that overlap the geometry are easy to generate, and the elements in the grid are regular shaped and undistorted. A numerical example is presented to demonstrate that the proposed solution structure accurately models the solution across material interface, and convergence analysis is performed to show that the method converges as the grid density is increased. Fiber reinforced microstructures are analyzed to compute the effective elastic properties using both 2D and 3D models to show that the results match closely with the ones available in the literature.

1. Introduction

The finite element method (FEM) is a well established numerical method for solution of engineering analysis problems and has been used extensively in micromechanical analysis of composite microstructures to determine effective properties (Sun and Vaidya, 1996; Taliercio, 2005; Xia et al., 2003; Marrey and Sankar, 1997; Zhu et al., 1998). The effective elastic properties are determined by performing six different analyses on the representative volume element (RVE) of the composite. In each of the analysis, one of the six macro-strains (average strain over the RVE) is kept non-zero while the remaining five macro-strains are set to zero. This is accomplished by imposing appropriate periodic boundary conditions on the outer surfaces of the RVE. The mesh is generated in such a way that the element boundaries conform to the matrix–inclusion interfaces. However, for complicated microstructures, automatic mesh generation becomes difficult and special techniques and algorithms need to be developed (Kim and Swan, 2003) to generate a quality mesh with quadrilateral or hexahedral elements. Automatic mesh generation algorithms are available that work acceptably for most 2D problems but can be unreliable for some 3D geometries often resulting in poor or distorted elements in some regions that can lead to large error in the solution. Significant amount of user intervention is sometimes needed to correct such problems. For example, in the analysis of composite microstructures involved in textile composites, the automatic mesh generation often becomes difficult and one of the main problems is meshing the interfacial region as shown in Kim and Swan (2003). This region is multiply connected, posing difficulties in mesh generation. Furthermore, to impose periodic boundary conditions using multipoint constraints, it is convenient to ensure that there is a one-to-one correspondence between nodes on the opposite faces of the RVE. This requirement adds further difficulties to the mesh generation process.

In order to avoid these problems associated with the mesh generation process, several meshless techniques have been developed in the past two decades. Some of the popular meshless techniques include Element Free Galerkin Method (Belytschko et al., 1994, 1996), Meshless Local Petrov–Galerkin Method (Atluri and Zhu, 1998), Method of Finite Spheres (De and Bathe, 2000), Method of hp Clouds (Oden et al., 1998) and Natural Element Method (Sukumar et al., 2001). These methods differ from each other in the choice of basis functions, numerical integration schemes, weak form employed or the techniques used for imposing essential boundary conditions. Element Free Galerkin Method has been extended to incorporate discontinuous derivatives (Cai and Zhu, 2004; Cordes and Moran, 1996; Krongauz and Belytschko, 1998) for application to multi-material problems. Similarly, MLPG method has also been extended to incorporate material discontinuity

* Corresponding author. Tel.: +1 352 392 0816; fax: +1 352 392 1071.
E-mail address: akumar@ufl.edu (A.V. Kumar).

0020-7683/$ - see front matter © 2009 Elsevier Ltd. All rights reserved.
doi:10.1016/j.ijsolstr.2009.02.003

and enable micromechanical analysis (Dang and Sankar, 2007). An alternative to meshless methods is structured grid based methods for analysis that avoid the need for a mesh that conforms to the geometry and interface boundaries. Extended finite element method or X-FEM developed by Belytschko (Belytschko et al., 2003) is one such method that uses implicit equations for definition of the geometry of the analysis domain, and the essential boundary conditions are applied using Lagrange multipliers. Another approach for applying boundary condition for structured grid based analysis involves using implicit equations to construct solution structures that are designed to automatically satisfy the essential boundary conditions (Kantorovich and Krylov, 1958; Shapiro and Tsukanov, 1999; Höllig, 2003; Kumar et al., 2007). An implicit equation of a curve/surface is an equation of the form $\phi(\mathbf{x}) = 0$, which divides the space (a line in one-dimension, a plane in two-dimensions, and 3D space in three-dimensions) into two half-spaces. The first half-space given be $\phi(\mathbf{x}) > 0$ could be considered the inside of the solid region and the other half-space $\phi(\mathbf{x}) < 0$ will then be considered the outside of the solid region. The scalar function $\phi(\mathbf{x})$ is often referred to as the characteristic function. Shapiro (Shapiro and Tsukanov, 1999) and Höllig (Höllig, 2003) also use structured grids for the analysis where they use specialized implicit equations (termed R-functions) to define the boundaries. A structured grid is much easier to generate as compared to a finite element mesh and all the elements in the grid have regular geometry. However, the nodes are not guaranteed to lie on the boundary, this necessitates the use of special techniques for imposing boundary conditions. Kumar et al. (2007) have developed implicit boundary method for applying boundary conditions for analysis using a structured grid where approximate step functions are used to construct solution structures that satisfy boundary conditions.

In this paper, an extended finite element method is developed for micromechanical analysis in which implicit boundary method is used to ensure that interface conditions are satisfied. The implicit boundary method involves using approximate step functions to construct solution structures that allow discontinuous gradients across the interface boundary even though there may not be any nodes of the grid on this boundary. The representative volume element for many microstructures is a rectangle/cuboid and hence a structured grid can always be constructed such that nodes are present on the RVE boundaries. This feature is exploited to incorporate periodic boundary conditions using the classical techniques of multipoint constraints (Cook et al., 2003). For 2D problems, plane strain formulation is used to determine the transverse elastic and shear moduli and the corresponding Poisson's ratios; generalized plane strain formulation (Li and Lim, 2005) is used to determine the longitudinal elastic modulus and longitudinal shear moduli are determined by using longitudinal shear formulation as described by Adams and Crane (1984) and Zhu et al. (1998). However for 3D problems, no idealization is necessary and all the elastic and shear moduli are determined by 3D stress formulation. The rest of the paper is organized as follows: In Section 2, the solution structure constructed using step functions is presented along with the corresponding modified weak form for elastostatic problems. Methods for imposing periodic boundary conditions are presented in Section 3. Section 4 describes efficient numerical implementation scheme for computation of various terms in the modified weak form. Computation of effective properties based on plane strain, generalized plane strain and longitudinal shear strain conditions are presented in Section 5. Numerical examples are presented to demonstrate validity and convergence of the solution structure in Section 6. This section also presents examples in 2D and 3D to determine effective elastic properties. The results are compared with FEM and results available in the literature.

2. Solution structure for modeling material discontinuity

In the finite element method, the mesh is created such that the element edges/faces form the material interface boundary. When structured grids are used for analysis, the nodes may not lie on the material interface and hence there is challenge in imposing interface conditions for material discontinuity. A solution structure is described here that is obtained by blending together the solutions represented using two identical overlapping grids, corresponding to the matrix (grid 1) and the inclusion (grid 2), as shown in Fig. 1 where only the elements that contribute to the solution from each grid are shown.

If $\mathbf{u}^{\mathbf{g1}}$ and $\mathbf{u}^{\mathbf{g2}}$ are fields constructed by piecewise interpolation within the elements of grids 1 and 2, respectively, the solution structure for the displacement field within the RVE can be constructed as

$$\mathbf{u} = (1 - H^{inc})\mathbf{u}^{\mathbf{g1}} + H^{inc}\mathbf{u}^{\mathbf{g2}} \tag{1}$$

In the preceding equation, H^{inc} is an approximate step function of the inclusion which has a unit value within the inclusion and transitions sharply to zero at the boundary of the inclusion as shown in Fig. 2. We shall refer to this approximate step function as the inclusion function. Implicit equations of the boundaries of the inclusion material will be used to construct this approximate step function and used to blend the solution from the inclusion grid and matrix grid to form a solution structure as shown in Eq. (1).

Fig. 2 shows a plot of the inclusion function in one-dimension but an expression for this function can be constructed for arbitrary dimension using an implicit equation the interface boundary. Let $\phi(\mathbf{x}) = 0$ be the implicit equation of the interface boundary between two materials such that $\phi > 0$ represents the region occupied by the inclusion material. Then, an expression for the inclusion function can be constructed as follows:

$$H^{inc}(\phi) = \begin{cases} 0 & \phi \leqslant 0 \\ 1 - \left(1 - \frac{\phi}{\delta}\right)^k & 0 \leqslant \phi \leqslant \delta \\ 1 & \phi \geqslant \delta \end{cases} \tag{2}$$

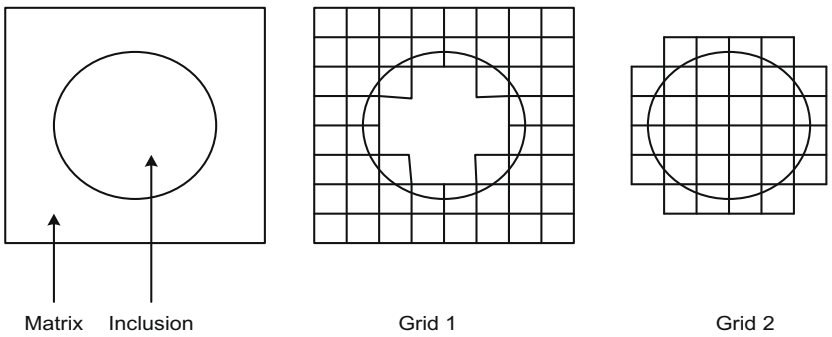

Fig. 1. Structured grids used to model matrix and inclusion.

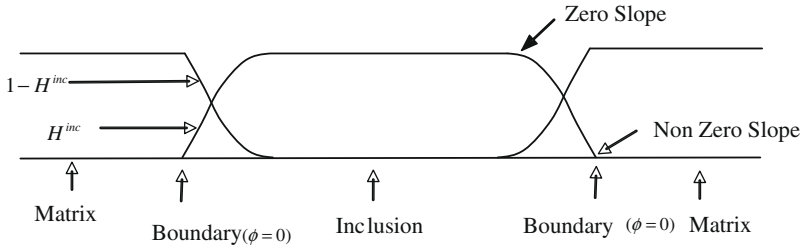

Fig. 2. Approximate step function of inclusion.

It can be seen that the inclusion function is unity inside the inclusion and transitions to zero at the boundary of the inclusion with a non-zero slope determined by the parameter δ. This function is a shifted approximate step function that tends to the Heaviside step function in the limit as $\delta \to 0$ but has a value of zero on the boundary unlike in traditional approximations of step functions where it has value of 0.5 (Osher and Fedkiw, 2002). Moreover, for allowing discontinuity in the normal strain, $H^{inc}(\phi)$ is constructed to have non-zero and discontinuous gradient at $\phi = 0$. At $\phi = \delta$ this function has C^{k-1} continuity. In this paper, the step function approximation of H^{inc} with $k = 2$ and very small value of δ is used as inclusion function with values of $\delta \approx 10^{-2}$ or smaller.

The solution structure in Eq. (1) combines the solution from both grids (Fig. 1) to represent the solution in the analysis domain. When the inclusion function is unity, the solution is given by $\mathbf{u} = \mathbf{u^{g2}}$, which is the solution from the inclusion part and when the inclusion function is zero, the solution is given by $\mathbf{u} = \mathbf{u^{g1}}$, which is the solution from the matrix. In the region where the inclusion function varies from zero to unity, the solution is a blend of the solutions from matrix grid and inclusion grid. This way of constructing solution structure ensures the displacement continuity of the solution through out the analysis domain. It also allows the normal strain to be discontinuous at the interface. This property can be seen from the gradients of the solution structure as shown below.

$$\frac{\partial u_i}{\partial x_j} = \left((1 - H^{inc}) \frac{\partial u_i^{g1}}{\partial x_j} - \frac{\partial H^{inc}}{\partial x_j} u_i^{g1} + H^{inc} \frac{\partial u_i^{g2}}{\partial x_j} + \frac{\partial H^{inc}}{\partial x_j} u_i^{g2} \right) \tag{3}$$

In this expression, the first term: $(1 - H^{inc}) \frac{\partial u_i^{g1}}{\partial x_j}$ and third term $H^{inc} \frac{\partial u_i^{g2}}{\partial x_j}$ are continuous at the interface boundary while the second term: $-\frac{\partial H^{inc}}{\partial x_j} u_i^{g1}$ and fourth term $\frac{\partial H^{inc}}{\partial x_j} u_i^{g2}$ are discontinuous at the interface boundary because $\frac{\partial H^{inc}}{\partial x_j}$ is zero for $\phi < 0$ and non-zero for $0 < \phi < \delta$. Therefore these terms provide independent slopes on the two sides of the interface allowing discontinuous normal strains when necessary and at the same time producing a continuous strain if $u_i^{g1} = u_i^{g2}$.

2.1. Modified weak form

The weak form of the elastostatic boundary value problem is the principle of virtual work which can be written in the following form:

$$\int_\Omega \{\delta\boldsymbol{\varepsilon}\}^{\mathbf{T}} \{\boldsymbol{\sigma}\}\, d\Omega = \int_{\Gamma_t} \{\delta\mathbf{u}\}^{\mathbf{T}} \{\mathbf{t}\}\, d\Gamma + \int_\Omega \{\delta\mathbf{u}\}^{\mathbf{T}} \{\mathbf{b}\}\, d\Omega \tag{4}$$

Here $\{\delta\boldsymbol{\varepsilon}\}$ is the virtual strain, $\{\boldsymbol{\sigma}\}$ is the Cauchy stress tensor, $\{\mathbf{t}\}$ is the traction vector, $\{\delta\mathbf{u}\}$ is the virtual displacement and $\{\mathbf{b}\}$ is the body force. For elastostatic problems, the essential boundary conditions are displacements $\{\mathbf{u}\} = \{\mathbf{u_0}\}$ specified on Γ_u and the natural boundary conditions are traction $\{\mathbf{t}\} = \{\mathbf{t_0}\}$ specified on Γ_t.

The displacements within the grid elements are interpolated as $u_i^{g1} = N_j u_{ij}^{g1}$ for the grid corresponding to matrix and $u_i^{g2} = N_j u_{ij}^{g2}$ for the inclusion grid where, N_j are the shape functions and u_{ij}^{g1} is the ith component of displacement for the jth node of the element. Then, based on the solution structure in Eq. (1), the displacement vector within an element can be expressed as:

$$\{\mathbf{u}\} = [\overline{\mathbf{N}}]\{\mathbf{X_e}\} = \begin{bmatrix} [\overline{\mathbf{N}}_\mathbf{1}] & [\overline{\mathbf{N}}_\mathbf{2}] \end{bmatrix} \begin{Bmatrix} \{\mathbf{X_{g1}}\} \\ \{\mathbf{X_{g2}}\} \end{Bmatrix} \tag{5}$$

where, the nodal displacement vector for the element, $\{\mathbf{X_e}\}$, is partitioned into nodal values from grid 1 and grid 2. $\{\mathbf{X_{g1}}\}$ are the nodal values corresponding to grid 1 and $\{\mathbf{X_{g2}}\}$ are the nodal values corresponding to grid 2. The matrices $[\overline{\mathbf{N}}_\mathbf{i}]$ can be expressed as:

$$[\overline{\mathbf{N}}_\mathbf{1}]^{\mathbf{T}} = (1 - H^{inc})[\mathbf{N}] \tag{6}$$

$$[\overline{\mathbf{N}}_\mathbf{2}]^{\mathbf{T}} = H^{inc}[\mathbf{N}] \tag{7}$$

$$[\mathbf{N}] = [\,[\mathbf{N_1}] \quad [\mathbf{N_2}] \quad \cdots \quad [\mathbf{N_n}]\,] \tag{8}$$

$$[\mathbf{N_i}] = \begin{bmatrix} N_i & 0 \\ 0 & N_i \end{bmatrix} \tag{9}$$

Similarly, the virtual displacements can be expressed as $\{\delta\mathbf{u}\} = [\overline{\mathbf{N}}]\{\delta\mathbf{X_e}\}$. The strains for 2D models can be computed for each element using the following expression:

$$\begin{Bmatrix} \varepsilon_1 \\ \varepsilon_2 \\ \gamma_{12} \end{Bmatrix} = \begin{Bmatrix} \dfrac{\partial u_1}{\partial x_1} \\ \dfrac{\partial u_2}{\partial x_2} \\ \dfrac{\partial u_1}{\partial x_2} + \dfrac{\partial u_2}{\partial x_1} \end{Bmatrix} = \begin{bmatrix} [\overline{\mathbf{B}}_\mathbf{1}] & [\overline{\mathbf{B}}_\mathbf{2}] \end{bmatrix} \begin{Bmatrix} \{\mathbf{X_{g1}}\} \\ \{\mathbf{X_{g2}}\} \end{Bmatrix} = \begin{bmatrix} [\overline{\mathbf{B}}_\mathbf{1}] & [\overline{\mathbf{B}}_\mathbf{2}] \end{bmatrix} \{\mathbf{X_e}\} \tag{10}$$

In the above expression, $[\overline{\mathbf{B}}] = [\,[\overline{\mathbf{B}}_1] \quad [\overline{\mathbf{B}}_2]\,]$ is the modified strain–displacement matrix and is a combination of strain–displacement matrices from the two grids. For the 2D strain vector in Eq. (10), the components of the strain–displacement matrix can be expressed as:

$$[\overline{\mathbf{B}}_\mathbf{1}] = (1 - H^{inc})[\mathbf{B}] - [\mathbf{H}][\mathbf{N}] \tag{11}$$

$$[\overline{\mathbf{B}}_2] = H^{inc}[\mathbf{B}] + [\mathbf{H}][\mathbf{N}] \tag{12}$$

where

$$[\mathbf{B}] = [\,[\mathbf{B_1}] \quad [\mathbf{B_2}] \quad \cdots \quad [\mathbf{B_n}]\,] \tag{13}$$

$$[\mathbf{B_i}] = \begin{bmatrix} \dfrac{\partial N_i}{\partial x_1} & 0 \\ 0 & \dfrac{\partial N_i}{\partial x_2} \\ \dfrac{\partial N_i}{\partial x_2} & \dfrac{\partial N_i}{\partial x_1} \end{bmatrix} \tag{14}$$

$$[\mathbf{H}] = \begin{bmatrix} \dfrac{\partial H^{inc}}{\partial x_1} & 0 \\ 0 & \dfrac{\partial H^{inc}}{\partial x_2} \\ \dfrac{\partial H^{inc}}{\partial x_2} & \dfrac{\partial H^{inc}}{\partial x_1} \end{bmatrix} \tag{15}$$

The expression for stress is given as $\sigma_i = C_{ij}\varepsilon_j$, where C_{ij} are the elasticity coefficients. In the computation of stress, the inclusion or matrix elasticity coefficients are used when the strains are evaluated in the inclusion or matrix region, respectively. The modified weak form takes the following discrete form when the above expressions for stress and strain are incorporated into the weak form:

$$\sum_{e=1}^{NE}\{\delta\mathbf{X}^e\}^{\mathbf{T}}\int_{\Omega_e}\left[\begin{array}{cc}[\overline{\mathbf{B}}_1] & [\overline{\mathbf{B}}_2]\end{array}\right]^{\mathbf{T}}[\mathbf{C}]\left[\begin{array}{cc}[\overline{\mathbf{B}}_1] & [\overline{\mathbf{B}}_2]\end{array}\right]\{\mathbf{X}^e\}\,d\Omega = \sum_{e=1}^{NE}\{\delta\mathbf{X}^e\}^{\mathbf{T}}\int_{\Omega_e}[\overline{\mathbf{N}}]^{\mathbf{T}}\{\mathbf{b}\}\,d\Omega + \sum_{e=1}^{NBE}\{\delta\mathbf{X}^e\}^{\mathbf{T}}\int_{\Gamma_t}[\overline{\mathbf{N}}]^{\mathbf{T}}\{\mathbf{t}\}d\Gamma \tag{16}$$

In this expression, the summation is over the number of elements (NE) and the number of boundary elements (NBE) in the grid used for analysis. As in the finite element method, these element matrices can be assembled to form global equations, where the left hand side terms form the stiffness matrix and the right hand side the force vector.

3. Periodic boundary conditions

The inhomogeneous composite material can be assumed to be made of infinite number of periodic arrangement of identical cells such that its behavior can be predicted by analyzing the behavior of one of the cells. When the material is not periodic then it is often possible to define a representative volume element (RVE) if the material is homogenous at a macro-scale. In order to analyze the behavior at the micro-scale, the RVE is analyzed with appropriate loading and boundary conditions. The RVEs tile the computational domain by translation such that the neighboring cells must fit into each other in both deformed and un-deformed states. Hence the boundary conditions for the RVE should be periodic in order to preserve the continuity of displacements, strains and stresses across each RVE. The periodic boundary conditions are expressed as linear constraints and they are implemented as multipoint constraints in the finite element method. The following figure shows the necessity of periodic boundary conditions. It can be seen that deformation of the edges (faces) should be periodic to preserve continuity.

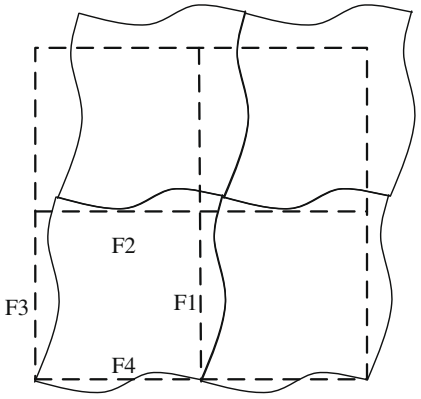

Fig. 3. Un-deformed and deformed configuration of a set of 4 RVEs.

The periodic boundary conditions are expressed in the following form:

$$u_{F_1} - u_{F_3} = const \text{ or in general } u_{F_1} - \lambda_1 u_{F_3} + \mu_1 = 0 \tag{17a}$$

$$u_{F_2} - u_{F_4} = const \text{ or in general } u_{F_2} - \lambda_2 u_{F_4} + \mu_2 = 0 \tag{17b}$$

In the preceding equation, u_{F_1} and u_{F_3} are displacement component at corresponding points on the opposing faces F_1 and F_3, respectively, as shown in Fig. 3. Similarly, u_{F_2} and u_{F_4} are displacement component on faces F_2 and F_4 and λ_i and μ_i are constants. The multipoint constraints were implemented exactly as is done in traditional finite element method (Cook et al., 2003). Structured grid with elements that use Lagrange interpolations functions were used for all the examples in this paper. Rectangular or cuboid RVE were uniformly divided to generate the grid such that identical nodes are present on all the edges/faces of the RVE to facilitate the imposition of periodic boundary conditions. This is obviously easier to accomplish for structured grids than for finite element mesh because it is not necessary to have nodes on interface boundaries and identical grid nodes are automatically present on opposite faces of the RVE. Fig. 4 shows a typical RVE used to model the microstructure of fiber reinforced composite where the coordinate system is chosen such the x_1 direction corresponds to the fiber direction. The figure also shows the naming convention used to refer to the various faces of the RVE.

Table 1 shows the periodic boundary conditions needed on the various faces of the RVE to impose six independent unit macro-

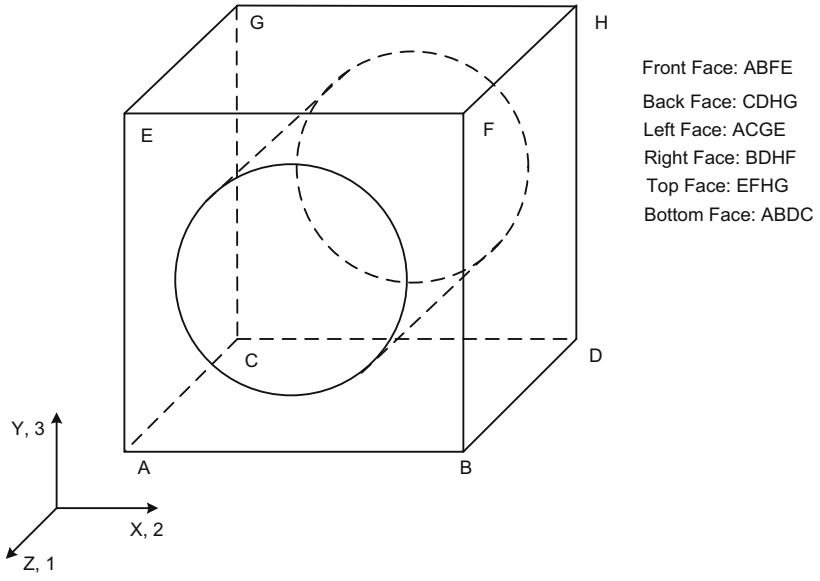

Fig. 4. Representative volume element used for computation of effective properties of a unidirectional fiber composite.

Table 1
Periodic boundary conditions for the six independent macro-strains.

Case	Unit strain	Front and back face	Left and right face	Top and bottom face
1	ε_{11}	$u_1^f = u_1^{bk} + L;\ u_2^f = u_2^{bk};\ u_3^f = u_3^{bk}$	$u_1^r = u_1^l;\ u_2^r = u_2^l;\ u_3^r = u_3^l$	$u_1^t = u_1^b;\ u_2^t = u_2^b;\ u_3^t = u_3^b$
2	ε_{22}	$u_1^f = u_1^{bk};\ u_2^f = u_2^{bk};\ u_3^f = u_3^{bk}$	$u_1^r = u_1^l;\ u_2^r = u_2^l + L;\ u_3^r = u_3^l$	$u_1^t = u_1^b;\ u_2^t = u_2^b;\ u_3^t = u_3^b$
3	ε_{33}	$u_1^f = u_1^{bk};\ u_2^f = u_2^{bk};\ u_3^f = u_3^{bk}$	$u_1^r = u_1^l;\ u_2^r = u_2^l;\ u_3^r = u_3^l$	$u_1^t = u_1^b;\ u_2^t = u_2^b;\ u_3^t = u_3^b + L$
4	γ_{23}	$u_1^f = u_1^{bk};\ u_2^f = u_2^{bk};\ u_3^f = u_3^{bk}$	$u_1^r = u_1^l;\ u_2^r = u_2^l;\ u_3^r = u_3^l + L$	$u_1^t = u_1^b;\ u_2^t = u_2^b;\ u_3^t = u_3^b$
5	γ_{13}	$u_1^f = u_1^{bk};\ u_2^f = u_2^{bk};\ u_3^f = u_3^{bk} + L$	$u_1^r = u_1^l;\ u_2^r = u_2^l;\ u_3^r = u_3^l$	$u_1^t = u_1^b;\ u_2^t = u_2^b;\ u_3^t = u_3^b$
6	γ_{12}	$u_1^f = u_1^{bk};\ u_2^f = u_2^{bk};\ u_3^f = u_3^{bk}$	$u_1^r = u_1^l;\ u_2^r = u_2^l;\ u_3^r = u_3^l$	$u_1^t = u_1^b + L;\ u_2^t = u_2^b;\ u_3^t = u_3^b$

strain components. In the table, u_i^f stands for the ith displacement component on the front face. Similarly, the superscripts: *bk*, *r*, *l*, *t* and *b* are used for back, right, left, top and bottom faces of the RVE. The RVE is assumed to be a cube of side length L.

The nodes on the faces (or edges in 2D) of the RVE can be partitioned into two parts: independent or master nodes ($\mathbf{m}$) and dependent or slave nodes ($\mathbf{s}$). The displacement vector can be similarly partitioned into $\mathbf{u} = [\mathbf{u_m u_s}]$, where $\mathbf{u_m}$ are displacement of the master nodes and $\mathbf{u_s}$ are those of slave nodes. The displacements for the slave nodes are specified in terms of the master nodes in the following form $\mathbf{u_s = G_1 u_m + g1}$, where $\mathbf{g1}$ is the non-zero periodic boundary conditions (e.g., Case 1: $u_1^f = u_1^{bk} + L$). Hence the displacements are expressed as:

$$\mathbf{u} = \begin{bmatrix} \mathbf{u_m} \\ \mathbf{u_s} \end{bmatrix} = \begin{bmatrix} \mathbf{I} \\ \mathbf{G_1} \end{bmatrix} [\mathbf{u_m}] + \begin{bmatrix} \mathbf{0} \\ \mathbf{g1} \end{bmatrix} = \mathbf{G}[\mathbf{u_m}] + \mathbf{g} \tag{18}$$

where $\mathbf{I}$ denotes the identity matrix and $\mathbf{0}$ is the zero vector. The matrices $\mathbf{G}$ and $\mathbf{g}$ are constructed globally for all the master degrees of freedom present in the analysis model. Using this expression for displacement and a similar expression of the corresponding virtual displacement $\boldsymbol{\delta u = G[\delta u_m]}$ in the weak form, the global stiffness matrix is transformed into $\mathbf{K' = G^T K G}$ and the load vector is increased by $-\mathbf{G^T K g}$ to impose the multipoint constraints. It is to be noted that in a general case of multipoint constraints, $\mathbf{G}$ and $\mathbf{g}$ are constructed such that they may be a fully populated matrix and vector, respectively. However, when structured grids are used for analysis, identical nodes are guaranteed to be present on the opposite faces and hence with proper choice of node numbers, $\mathbf{G}$ matrix can be constructed to be a diagonal matrix. This simplifies the computations involved in the transformation of the stiffness matrix and hence leads to efficient implementation.

4. Numerical implementations

The solution structure presented in the previous section is such that the contribution from the matrix grid is suppressed by the inclusion function within the inclusion and similarly the solution from inclusion grid does not contribute to the solution outside the inclusion. Therefore, the elements of the matrix grid that are completely inside the inclusion and the elements of the inclusion grid that are entirely outside the inclusion can be removed from the analysis by setting to zero the nodal values of nodes that belong only to these elements. This leads to a reduction in the total number of degrees of freedom for the analysis model. Furthermore, only the elements through which the interface boundary passes will have active overlapping elements from both the grids.

The strain–displacement matrix was decomposed into two parts $[\overline{\mathbf{B}}_1]$ and $[\overline{\mathbf{B}}_2]$ that correspond to the overlapping matrix and inclusion grid elements, respectively. These matrices were further decomposed into the part that depends on the gradient of the shape functions $[\mathbf{B}]$ and the part that depends on the gradient of the inclusion function $[\mathbf{H}]$. It can be noticed that some of these components of the strain–displacement matrix vanish in certain regions of the computational domain and are non-zero in other parts of computational domain depending on where the inclusion function and its gradients vanish. Therefore, the elements in the grid are divided into three types: elements that are in the matrix region, elements that are in the inclusion region and those that contain the interface region as shown in Fig. 5.

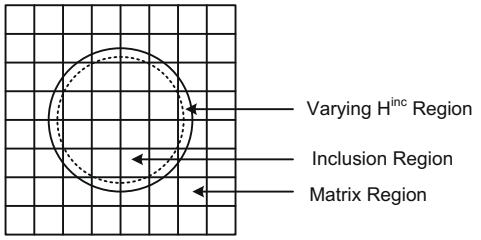

Fig. 5. Division of computational domain into three regions.

Matrix region: For elements that are in the matrix region, only the degrees of freedom for grid corresponding to matrix are active, therefore the strain–displacement matrix becomes $[\overline{\mathbf{B}}] = \begin{bmatrix} [\overline{\mathbf{B}}_1] & [\overline{\mathbf{B}}_2] \end{bmatrix} = \begin{bmatrix} [\mathbf{B}] & \mathbf{0} \end{bmatrix}$ because $H^{inc} = 0$ everywhere in the matrix. Therefore, the stiffness matrix will take the following form in matrix region:

$$[\mathbf{K}] = \int_{\Omega_e} \begin{bmatrix} [\overline{\mathbf{B}}_1] & [\overline{\mathbf{B}}_2] \end{bmatrix}^{\mathbf{T}} [\mathbf{C^{mat}}] \begin{bmatrix} [\overline{\mathbf{B}}_1] & [\overline{\mathbf{B}}_2] \end{bmatrix} dV = \int_{\Omega_e} \begin{bmatrix} [\mathbf{B}]^{\mathbf{T}} [\mathbf{C^{mat}}] [\mathbf{B}] & \mathbf{0} \\ \mathbf{0} & \mathbf{0} \end{bmatrix} dV \tag{19}$$

Inclusion region: In this region the degrees of freedom for grid corresponding to inclusion are active. The strain–displacement matrix becomes $[\overline{\mathbf{B}}] = \begin{bmatrix} [\overline{\mathbf{B}}_1] & [\overline{\mathbf{B}}_2] \end{bmatrix} = \begin{bmatrix} \mathbf{0} & [\mathbf{B}] \end{bmatrix}$ because $H^{inc} = 1$ everywhere within the inclusion. The stiffness matrix is expressed as:

$$[\mathbf{K}] = \int_{\Omega_e} \begin{bmatrix} [\overline{\mathbf{B}}_1] & [\overline{\mathbf{B}}_2] \end{bmatrix}^{\mathbf{T}} [\mathbf{C^{inc}}] \begin{bmatrix} [\overline{\mathbf{B}}_1] & [\overline{\mathbf{B}}_2] \end{bmatrix} dV = \int_{\Omega_e} \begin{bmatrix} \mathbf{0} & \mathbf{0} \\ \mathbf{0} & [\mathbf{B}]^{\mathbf{T}} [\mathbf{C^{inc}}] [\mathbf{B}] \end{bmatrix} dV \tag{20}$$

Interface region: In this region, the approximate step function transitions from zero to unity. Elements from both grids contribute to the solutions within the element and strain–displacement matrix becomes $[\overline{\mathbf{B}}] = \begin{bmatrix} [\overline{\mathbf{B}}_1] & [\overline{\mathbf{B}}_2] \end{bmatrix}$. The stiffness matrix is expressed as:

$$\begin{aligned} [\mathbf{K}] &= \int_{\Omega_e} \begin{bmatrix} [\overline{\mathbf{B}}_1] & [\overline{\mathbf{B}}_2] \end{bmatrix}^{\mathbf{T}} [\mathbf{C}] \begin{bmatrix} [\overline{\mathbf{B}}_1] & [\overline{\mathbf{B}}_2] \end{bmatrix} dV \\ &= \int_{\Omega_e} \begin{bmatrix} [\overline{\mathbf{B}}_1]^{\mathbf{T}} [\mathbf{C}] [\overline{\mathbf{B}}_1] & [\overline{\mathbf{B}}_1]^{\mathbf{T}} [\mathbf{C}] [\overline{\mathbf{B}}_2] \\ [\overline{\mathbf{B}}_2]^{\mathbf{T}} [\mathbf{C}] [\overline{\mathbf{B}}_1] & [\overline{\mathbf{B}}_2]^{\mathbf{T}} [\mathbf{C}] [\overline{\mathbf{B}}_2] \end{bmatrix} dV = \begin{bmatrix} [\mathbf{K_{11}}] & [\mathbf{K_{12}}] \\ [\mathbf{K_{21}}] & [\mathbf{K_{22}}] \end{bmatrix} \end{aligned} \tag{21}$$

In this expression $[\mathbf{C}] = [\mathbf{C^{inc}}]$ or $[\mathbf{C^{mat}}]$ depending on which region is being integrated upon. Each of the terms in this matrix can be decomposed as a sum of volume integral and a surface integral. The procedure for this decomposition is described in detail for $[\mathbf{K_{11}}]$.

$$[\mathbf{K_{11}}] = \int_{\Omega_e} [\overline{\mathbf{B}}_1]^{\mathbf{T}} [\mathbf{C}] [\overline{\mathbf{B}}_1] \, d\Omega = \left[\mathbf{K_{11}^{(1)}}\right] + \left[\mathbf{K_{11}^{(2)}}\right] + \left[\mathbf{K_{11}^{(3)}}\right] + \left[\mathbf{K_{11}^{(4)}}\right] \tag{22}$$

Substituting the definition of $\overline{\mathbf{B}}_1$ from Eq. (11), we get,

$$
\begin{aligned}
[\mathbf{K}_{11}^{(1)}] &= \int_{\Omega_e}\{(1-H^{inc})^2[\mathbf{B}]^{\mathbf{T}}[\mathbf{C}][\mathbf{B}]\}\,dV \\
[\mathbf{K}_{11}^{(2)}] &= \int_{\Omega_e}\{(1-H^{inc})[\mathbf{B}]^{\mathbf{T}}[\mathbf{C}][\mathbf{H}][\mathbf{N}]\}\,dV \\
[\mathbf{K}_{11}^{(3)}] &= \int_{\Omega_e}\{(1-H^{inc})[\mathbf{N}]^{\mathbf{T}}[\mathbf{H}]^{\mathbf{T}}[\mathbf{C}][\mathbf{B}]\}\,dV \\
[\mathbf{K}_{11}^{(4)}] &= \int_{\Omega_e}\{[\mathbf{N}]^{\mathbf{T}}[\mathbf{H}]^{\mathbf{T}}[\mathbf{C}][\mathbf{H}][\mathbf{N}]\}\,dV
\end{aligned}
\tag{23}
$$

In this expression, the first term $[\mathbf{K}_{11}^{(1)}]$ is non-zero only outside the inclusion where $H^{inc} = 0$. The integration to compute this component is performed by subdividing the element into triangles or tetrahedra. The remaining three terms $[\mathbf{K}_{11}^{(2)}]$, $[\mathbf{K}_{11}^{(3)}]$ and $[\mathbf{K}_{11}^{(4)}]$ include the matrix $[\mathbf{H}]$ which contains gradients of the approximate step function. Therefore, these terms are non-zero only in the thin band along the interface boundary in which the gradient of the inclusion function is non-zero. This allows the volume integral to be converted to a surface integral by using very small value of the range parameter δ in Eq. (2). The gradients of inclusion function has large magnitude within this band when δ is made very small so its contribution to the integral cannot be ignored even though the band is very narrow. The integral can be converted into a surface integral by performing a change of coordinates to t, n (tangent and normal to the boundary) as shown in Fig. 6 and computing the integral in the normal direction analytically. The integral in the normal direction is evaluated using the assumption that only quantities that are a function of the inclusion function $H^{inc}(\phi)$ and its gradients vary across the band and all other quantities are constant in the normal direction. A change of variable from spatial coordinate n to the characteristic function ϕ makes this integral easy to evaluate as shown below where an arbitrary function $f(\phi)$ is integrated across the band whose width is $n_2 - n_1$.

$$
\int_{n_1}^{n_2} f(\phi)\,dn = \int_0^{\delta} f(\phi)\frac{1}{|\nabla\phi|}\,d\phi \tag{24}
$$

Using the approach described above the last three terms in Eq. (23) can be converted to surface integrals as shown below:

$$
\begin{aligned}
\left[\mathbf{K}_{11}^{(2)}\right] &= \int_{\Gamma}\left\{[\mathbf{B}]^{\mathbf{T}}\left(\int_{\phi}(1-H^{inc})[\mathbf{C}][\mathbf{H}]\frac{1}{|\nabla\phi|}\,d\phi\right)[\mathbf{N}]\right\}dt \\
\left[\mathbf{K}_{11}^{(3)}\right] &= \int_{\Gamma}\left\{[\mathbf{N}]^{\mathbf{T}}\left(\int_{\phi}(1-H^{inc})[\mathbf{H}]^{\mathbf{T}}[\mathbf{C}]\frac{1}{|\nabla\phi|}\,d\phi\right)[\mathbf{B}]\right\}dt \\
\left[\mathbf{K}_{11}^{(4)}\right] &= \int_{\Gamma}\left\{[\mathbf{N}]^{\mathbf{T}}\left(\int_{\phi}[\mathbf{H}]^{\mathbf{T}}[\mathbf{C}][\mathbf{H}]\frac{1}{|\nabla\phi|}\,d\phi\right)[\mathbf{N}]\right\}dt
\end{aligned}
\tag{25}
$$

The matrices $[\mathbf{B}]$ and $[\mathbf{N}]$ are treated as constants and taken out of the inner integral but they are not constants for the outer integral which is along the boundary. This decomposition leads to efficient and accurate computation of the stiffness matrix. Using the same approach, the other components of the stiffness matrix can be evaluated as:

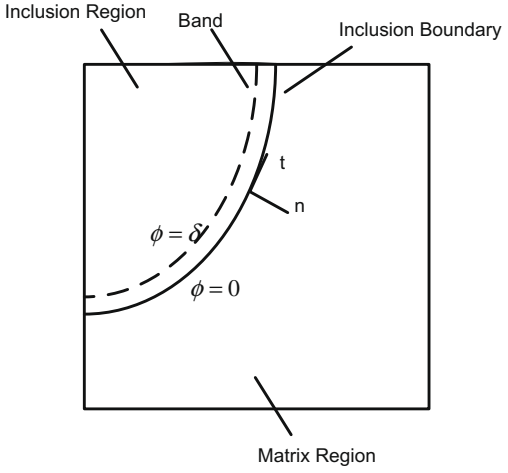

Fig. 6. Band with varying inclusion function.

$$
[\mathbf{K}_{22}] = \left[\mathbf{K}_{22}^{(1)}\right] + \left[\mathbf{K}_{22}^{(2)}\right] + \left[\mathbf{K}_{22}^{(3)}\right] + \left[\mathbf{K}_{22}^{(4)}\right] \tag{26}
$$

Using the definition of $\overline{\mathbf{B}}_2$ and converting volume integrals into surface integrals when possible, we get,

$$
\begin{aligned}
\left[\mathbf{K}_{22}^{(1)}\right] &= \int_{\Omega_e}\left\{[\mathbf{B}]^{\mathbf{T}}\left(\int_{\phi}\left(H^{inc}\right)^2[\mathbf{C}]\frac{1}{|\nabla\phi|}\,d\phi\right)[\mathbf{B}]\right\}dV \\
\left[\mathbf{K}_{22}^{(2)}\right] &= \int_{\Gamma}\left\{[\mathbf{B}]^{\mathbf{T}}\left(\int_{\phi}H^{inc}[\mathbf{C}][\mathbf{H}]\frac{1}{|\nabla\phi|}\,d\phi\right)[\mathbf{N}]\right\}dt \\
\left[\mathbf{K}_{22}^{(3)}\right] &= \left[\mathbf{K}_{22}^{(2)}\right]^{\mathbf{T}} \\
\left[\mathbf{K}_{22}^{(4)}\right] &= \left[\mathbf{K}_{11}^{(4)}\right]^{\mathbf{T}}
\end{aligned}
\tag{27}
$$

Similarly, the off-diagonal terms ($[\mathbf{K}_{12}] = [\mathbf{K}_{21}]^{\mathbf{T}}$) can be evaluated as shown below. Any component containing $H^{inc}(1 - H^{inc})$ is neglected since this term will be zero in both the inclusion and the matrix and has small magnitude along the boundary band.

$$
[\mathbf{K}_{12}] = [\mathbf{K}_{21}]^{\mathbf{T}} = \left[\mathbf{K}_{11}^{(2)}\right] - \left[\mathbf{K}_{22}^{(3)}\right] - \left[\mathbf{K}_{11}^{(4)}\right] \tag{28}
$$

5. Computation of effective properties

Effective properties of the composite materials with periodic distribution of microstructures are computed by applying far-field (macro) strains to the RVE. The displacements, strains and stresses are assumed to be periodic in the RVE. Hill's lemma (Qu and Cherkaoui, 2006) states that the average of the strain energy in RVE is same as the strain energy due to average stress and strains. It can be stated in the form $\langle\boldsymbol{\sigma}:\boldsymbol{\varepsilon}\rangle = \langle\boldsymbol{\sigma}\rangle:\langle\boldsymbol{\varepsilon}\rangle$, where $\langle\mathbf{a}\rangle = \frac{1}{V}\int_V \mathbf{a}\,dV$ represents the average value of $\mathbf{a}$ over the volume V of the RVE. This property is used to compute the effective properties from an RVE. The average stresses and strains are computed by solving the boundary value problem six times with different applied strains. These average stresses and strains are used in the relation $\langle\boldsymbol{\sigma}\rangle = \mathbf{C}^{\mathbf{H}}\langle\boldsymbol{\varepsilon}\rangle$ or its inverse $\langle\boldsymbol{\varepsilon}\rangle = \mathbf{S}^{\mathbf{H}}\langle\boldsymbol{\sigma}\rangle$ to determine a row (or column) of the homogenized stiffness matrix $\mathbf{C}^{\mathbf{H}}$ (or $\mathbf{S}^{\mathbf{H}}$). In this paper, six different unit strain states were used to determine all the components of $\mathbf{S}^{\mathbf{H}}$. The strain–stress relation for orthotropic materials in the form $\langle\boldsymbol{\varepsilon}\rangle = \mathbf{S}^{\mathbf{H}}\langle\boldsymbol{\sigma}\rangle$ is as follows:

$$
\begin{Bmatrix}\varepsilon_{11}\\ \varepsilon_{22}\\ \varepsilon_{33}\\ \gamma_{23}\\ \gamma_{31}\\ \gamma_{12}\end{Bmatrix} =
\begin{bmatrix}
\frac{1}{E_1} & -\frac{\nu_{21}}{E_2} & -\frac{\nu_{31}}{E_3} & 0 & 0 & 0\\
-\frac{\nu_{12}}{E_1} & \frac{1}{E_2} & -\frac{\nu_{32}}{E_3} & 0 & 0 & 0\\
-\frac{\nu_{13}}{E_1} & -\frac{\nu_{23}}{E_2} & \frac{1}{E_3} & 0 & 0 & 0\\
0 & 0 & 0 & \frac{1}{G_{23}} & 0 & 0\\
0 & 0 & 0 & 0 & \frac{1}{G_{31}} & 0\\
0 & 0 & 0 & 0 & 0 & \frac{1}{G_{12}}
\end{bmatrix}
\begin{Bmatrix}\sigma_{11}\\ \sigma_{22}\\ \sigma_{22}\\ \tau_{23}\\ \tau_{31}\\ \tau_{12}\end{Bmatrix}
\tag{29}
$$

In two-dimensional problems, the effective properties in the transverse directions are determined by analyzing the model in plane strain conditions. The longitudinal modulus is computed by analyzing the model in generalized plane strain conditions. The longitudinal shear moduli are computed by analyzing the model in longitudinal shear loading conditions. Each of these cases is explained in the following sub-sections.

6. Results and discussion

The implicit boundary method for modeling microstructures described in this paper was implemented by modifying a finite element program and will be referred to here as the Implicit Boundary

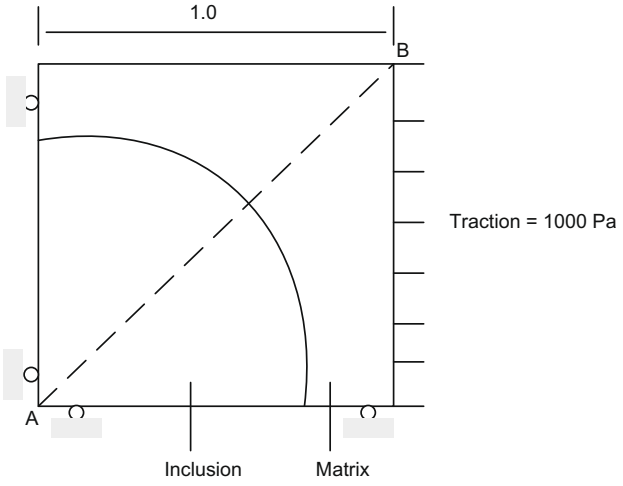

Fig. 7. Two material model used to validate solution structure.

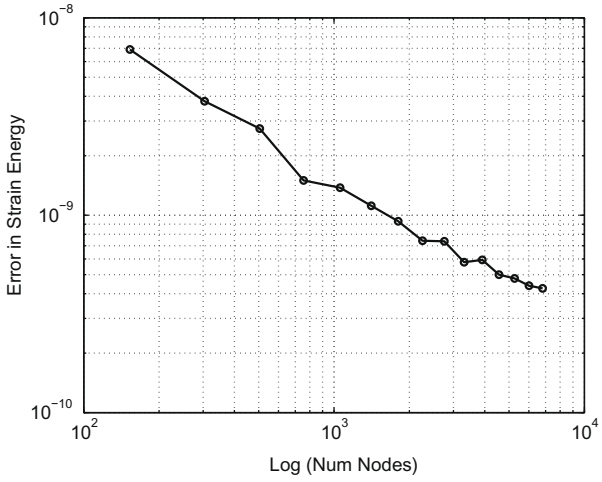

Fig. 9. Convergence plot for error in strain energy.

Finite Element Method (IBFEM). The shape of the inclusions was defined using implicit equations of its boundaries. These implicit equations were used for constructing the solution structure and for the computation of the stiffness matrix. The periodic boundary conditions were imposed using multipoint constraints. Several numerical examples are presented in this section to validate this approach. The first example is a square plate with a circular inclusion under axial tension. This problem demonstrates the validity of the solution structure for representing continuous displacements and discontinuous stress/strain across the interface boundaries. The second example involves computation of effective properties of a fiber reinforced composite using two-dimensional formulation and the third example involves the computation of the same properties using a three-dimensional model.

6.1. Example 6.1: square plate with a circular inclusion

This example demonstrates the validity of the solution structure presented in this paper. A circular inclusion of volume fraction $v_f = 0.47$ as shown in Fig. 7 is modeled in this example. Plane stress idealization was used assuming elastic properties of the matrix (aluminum) as: $E_m = 68.3$ GPa and $v_m = 0.3$ and the isotropic fiber material (boron) properties as: $E_f = 379.3$ GPa and $v_f = 0.1$. The solution obtained by IBFEM is compared with the solution obtained by FEM using ABAQUS software. The contour plot of stress in X-direction is plotted in Fig. 8 and it can be observed that the stress pattern as computed by FEM matches closely with the stress pattern as computed by IBFEM. The maximum and minimum values for the stresses also match very closely. Convergence analysis is performed by analyzing a sequence of models and the error in strain energy is plotted in Fig. 9. The solution from a highly dense FE model with 12,001 bi-quadratic quadrilateral elements was used as the exact solution for convergence analysis. The strain energy from the dense FE model was computed to be 4.273×10^{-6} J and the error in strain energy for a given grid density is computed as the difference in computed strain energy and the above value. It can be observed that the solution converges as the error approaches to zero when the grid density is increased.

The plots along the line AB are shown in Figs. 10 and 11. Fig. 10 shows the comparison of X-displacement along line AB (see Fig. 7) with FEM solution. It can be observed that the displacement solution obtained by IBFEM matches exactly with the FEM solution. A slope discontinuity can be observed at the inclusion boundary.

Fig. 11 shows the line plots of σ_{xx} and ε_{xx} along the line AB. Again, the solution for both stresses and strains match exactly with the FEM solution. The discontinuity in stress and strain can be observed at the inclusion interface.

6.2. Example 6.2: computation of effective properties using a two-dimensional model

In this example a two-dimensional model is used for computation of effective properties of a boron–aluminum fiber reinforced composite with a volume fraction of 0.47. Six different periodic boundary conditions are applied on the RVE as listed in Table 1. For determining the effective properties in the transverse direction,

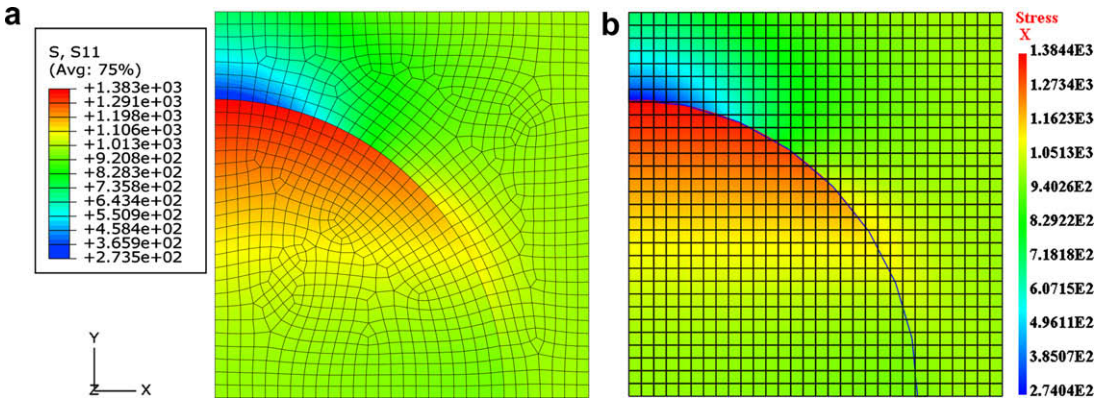

Fig. 8. Contour plot of X-stresses (a) FEM results (ABAQUS) (b) IBFEM results.

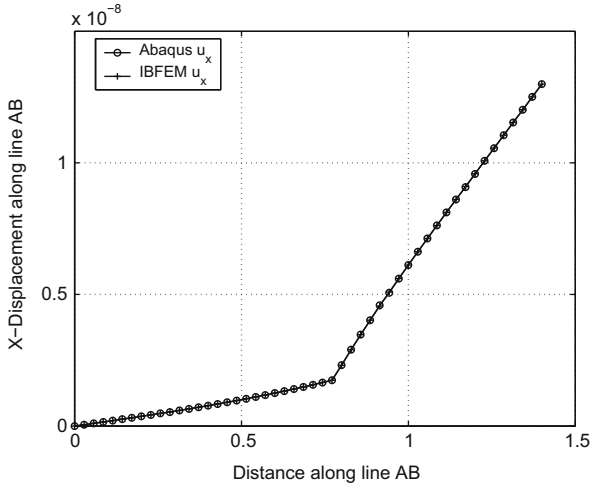

Fig. 10. Plot of *X*-displacements along line AB (as shown in Fig. 7).

plane strain assumption is used. The constitutive equation for plane strain is presented in the following equation.

$$\begin{Bmatrix}\sigma_x\\ \sigma_x\\ \tau_{xy}\end{Bmatrix} = \frac{E}{(1+v)(1-2v)}\begin{bmatrix}1-v & v & 0\\ v & 1-v & 0\\ 0 & 0 & \frac{1-2v}{2}\end{bmatrix}\begin{Bmatrix}\varepsilon_x\\ \varepsilon_y\\ \gamma_{xy}\end{Bmatrix} \tag{30}$$

This stress–strain relation is used in the modified weak form shown in Eq. (16) for Cases 2, 3 and 4 in Table 1 to solve the boundary value problem and compute the transverse material properties.

In order to determine the homogenized material properties in the longitudinal direction (Case 1 in Table 1), a generalized plane strain model (Li and Lim, 2005) is used. In this model, the strains in the longitudinal directions are specified. A constant strain in the z is assumed and the strains and stresses are expressed as follows:

$$\begin{Bmatrix}\varepsilon_x\\ \varepsilon_y\\ \varepsilon_z\\ \gamma_{xy}\end{Bmatrix} = \begin{Bmatrix}\frac{\partial u_x}{\partial x}\\ \frac{\partial u_y}{\partial y}\\ \bar{\varepsilon}_z\\ \frac{\partial u_x}{\partial y}+\frac{\partial u_y}{\partial x}\end{Bmatrix} \quad \text{and} \quad \begin{Bmatrix}\sigma_x\\ \sigma_y\\ \sigma_z\\ \tau_{xy}\end{Bmatrix} = \begin{bmatrix}C_{11} & C_{12} & C_{13} & 0\\ C_{21} & C_{22} & C_{23} & 0\\ C_{31} & C_{32} & C_{33} & 0\\ 0 & 0 & 0 & C_{66}\end{bmatrix}\begin{Bmatrix}\varepsilon_x\\ \varepsilon_y\\ \bar{\varepsilon}_z\\ \gamma_{xy}\end{Bmatrix} \tag{31}$$

Using the constant strain in z-direction, the stresses are written as follows:

$$\begin{Bmatrix}\sigma_x\\ \sigma_y\\ \tau_{xy}\end{Bmatrix} = \begin{bmatrix}C_{11} & C_{12} & 0\\ C_{12} & C_{22} & 0\\ 0 & 0 & C_{66}\end{bmatrix}\begin{Bmatrix}\varepsilon_x\\ \varepsilon_y\\ \gamma_{xy}\end{Bmatrix} + \begin{Bmatrix}C_{13}\\ C_{23}\\ 0\end{Bmatrix}\bar{\varepsilon}_z = [C]\{\varepsilon\} + C^k\bar{\varepsilon}_z$$
$$\text{and} \quad \sigma_z = [C_{13} \quad C_{23} \quad 0]\begin{Bmatrix}\varepsilon_x\\ \varepsilon_y\\ \gamma_{xy}\end{Bmatrix} + C_{33}\bar{\varepsilon}_z \tag{32}$$

The principle of virtual work (Eq. (16)) is modified by choosing the virtual strain vector as $\boldsymbol{\delta\varepsilon} = \{\delta\varepsilon_x \quad \delta\varepsilon_y \quad \delta\gamma_{xy}\}^T$ to get the following equation.

$$\int_\Omega \{\boldsymbol{\delta\varepsilon}\}^{\mathbf{T}}\{\boldsymbol{\sigma}\}\,d\Omega = \int_{\Gamma_t}\{\boldsymbol{\delta u}\}^{\mathbf{T}}\{\mathbf{t}\}\,d\Gamma + \int_\Omega \{\boldsymbol{\delta u}\}^{\mathbf{T}}\{\mathbf{b}\}\,d\Omega - \{\boldsymbol{\delta\varepsilon}\}^T C^k\bar{\varepsilon}_z \tag{33}$$

In this expression, the last term is the load due to prescribed strain in the third direction. The rest of the formulation is exactly similar to plane strain formulation. This model is used with unit strain in z-direction and periodic boundary conditions according to Case 1 in Table 1.

The homogenized shear properties in the longitudinal direction are determined by using a longitudinal shear loading (Cases 5 and 6 in Table 1), where there is only one degree of freedom which is the displacement in the z-direction. This assumption results in non-zero shear strains only in the $z-y$ and $z-x$ planes while all other strain and stress components are identically zero. The equations for shear strains and shear stress are given by the following expression:

$$\begin{Bmatrix}\gamma_{zy}\\ \gamma_{zx}\end{Bmatrix} = \begin{Bmatrix}\frac{\partial u_z}{\partial y}\\ \frac{\partial u_z}{\partial x}\end{Bmatrix} \quad \text{and} \quad \begin{Bmatrix}\sigma_{zy}\\ \sigma_{zx}\end{Bmatrix} = \begin{bmatrix}G_{zy} & 0\\ 0 & G_{zx}\end{bmatrix}\begin{Bmatrix}\gamma_{zy}\\ \gamma_{zx}\end{Bmatrix} \tag{34}$$

The principle of virtual work (Eq. (16)) is modified by choosing the virtual strain vector as $\boldsymbol{\delta\varepsilon} = \{\delta\gamma_{zy} \quad \delta\gamma_{zx}\}^T$. This formulation is used to specify unit shear strains (Cases 5 and 6) and compute the corresponding shear moduli.

The results obtained by IBFEM are compared with the results available in the literature (Sun and Vaidya, 1996; Sun and Chen, 1990; Chamis, 1984; Whitney and Riley, 1966). The periodic boundary conditions shown in Table 1 are used for the analysis. The average stresses for each case are tabulated in Table 2. Figs. 12–14 show the stress distribution for various cases with the deformed shape. The effective properties are computed by using the average stresses and strains and are compared in Table 3. It can be observed that the effective properties determined by the

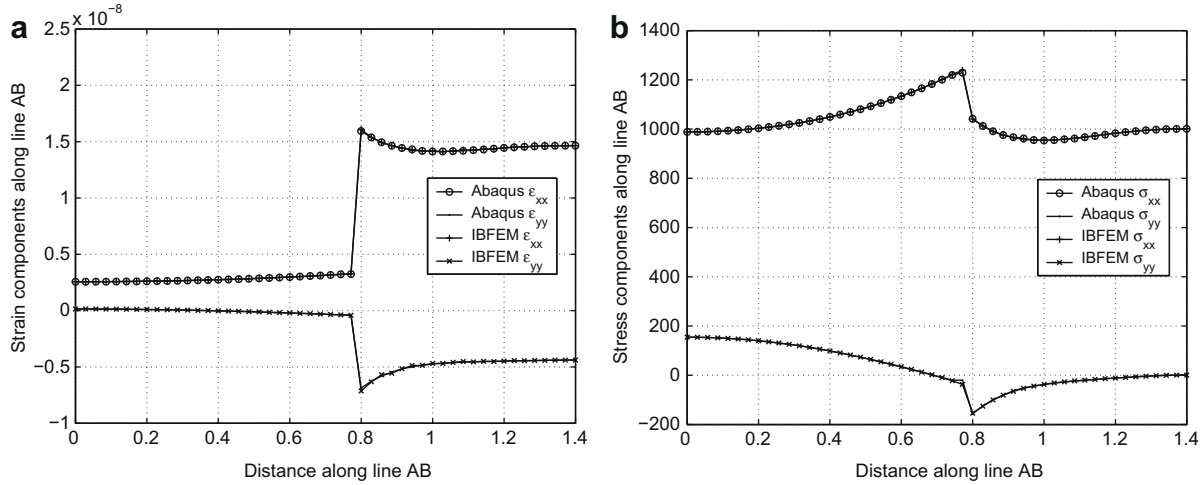

Fig. 11. (a) Comparison of σ_{xx} along line AB. (b) Comparison of ε_{xx} along line AB.

Table 2
State of stress for six different cases in 2D model.

Case	Unit strain	σ_{11}(GPa)	σ_{22}(GPa)	σ_{33}(GPa)	τ_{23}(GPa)	τ_{31}(GPa)	τ_{12}(GPa)
1	$\varepsilon_{11} = 1$	230.84	41.14	41.14	0	0	0
2	$\varepsilon_{22} = 1$	40.35	161.20	46.22	0	0	0
3	$\varepsilon_{33} = 1$	40.35	46.22	161.20	0	0	0
4	$\gamma_{23} = 1$	0	0	0	46.07	0	0
5	$\gamma_{31} = 1$	0	0	0	0	54.44	0
6	$\gamma_{12} = 1$	0	0	0	0	0	54.44

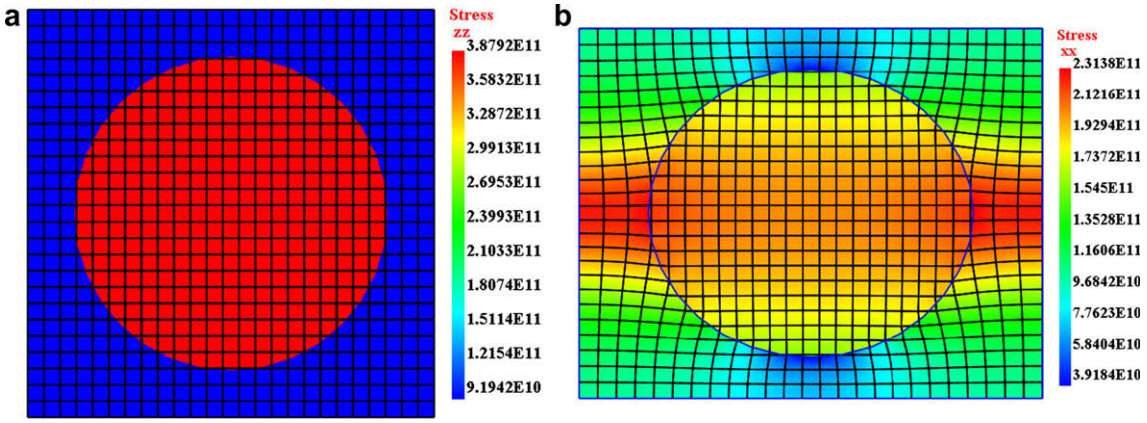

Fig. 12. (a) Plot of σ_{11} normal stress for Case 1 and (b) plot of σ_{22} normal stress for Case 2.

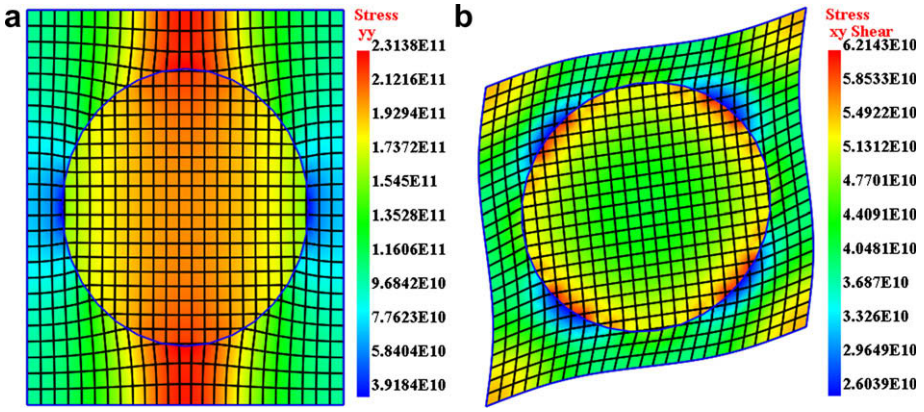

Fig. 13. (a) Plot of σ_{33} normal stress for Case 3 and (b) plot of τ_{23} shear stress for Case 4.

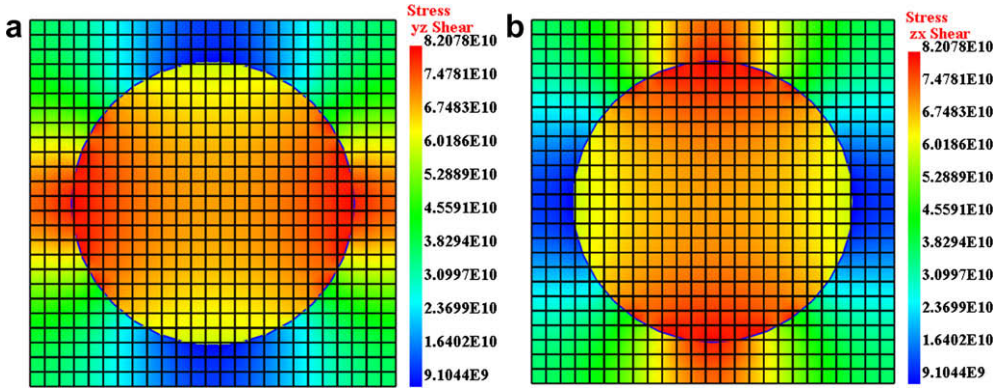

Fig. 14. (a) Plot of τ_{31} shear stress for Case 5 and (b) plot of τ_{12} shear stress for Case 6.

Table 3
Comparison of elastic effective properties obtained by IBFEM and the ones available in the literature.

Property	IBFEM 2D	IBFEM 3D	Ref: Sun and Vaidya (1996)	Ref: Sun and Chen (1990)	Ref: Chamis (1984)	Ref: Whitney and Riley (1966)
E_1(GPa)	214.83	214.85	215	214	214	215
E_2(GPa)	144.07	143.85	144	135	156	123
E_3(GPa)	144.07	143.85	144	135	156	123
G_{23}(GPa)	46.07	45.97	45.9	–	43.6	–
G_{13}(GPa)	54.44	54.35	57.2	51.1	62.6	53.9
G_{12}(GPa)	54.44	54.35	57.2	51.1	62.6	53.9
ν_{23}	0.25	0.25	0.29	–	0.31	–
ν_{13}	0.198	0.195				–
ν_{12}	0.198	0.195	0.19	0.19	0.20	0.19
ν_{32}	0.25	0.25				
ν_{31}	0.13	0.13				
ν_{21}	0.13	0.13				

current method match very closely with the effective elastic constants as reported in the literature.

To further test the method, the performance of the proposed solution structure is studied by increasing the fiber volume fraction to when the fiber boundary is tangential to the matrix boundary within the RVE. Several configurations are analyzed by increasing the fiber volume fraction from $0.80\frac{\pi}{4}$ to $\frac{\pi}{4}$. The plots of effective elastic moduli with increasing fiber volume fraction are shown in Fig. 15. It can be observed that the proposed method provides stable and expected behavior of elastic moduli with increasing fiber volume fraction.

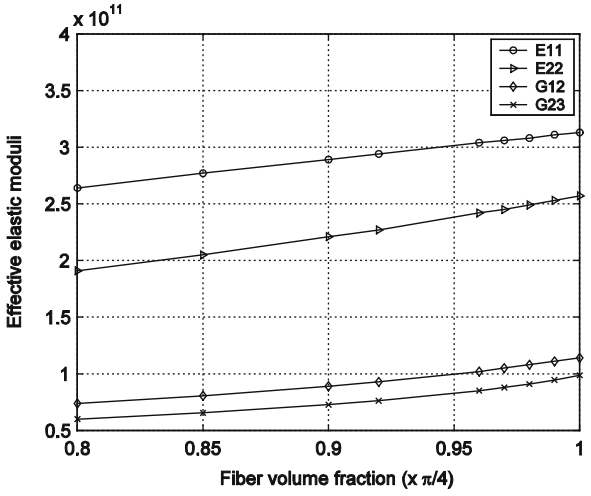

Fig. 15. Plot of elastic moduli versus fiber volume fraction.

Fig. 16 shows contour plots of a stress component for Cases 1 and 4 when the fiber volume fraction of fiber is $\frac{\pi}{4}$. For this volume fraction the effective properties were computed to be $E_1 = 313$ GPa, $E_2 = E_3 = 257$ GPa, $G_{23} = 99$ GPa, $G_{13} = G_{12} = 114$ GPa, $\nu_{23} = \nu_{32} = 0.174$, $\nu_{13} = \nu_{12} = 0.131$, $\nu_{31} = \nu_{21} = 0.108$. For comparison the longitudinal modulus computed using the rule of mixtures is $E_1 = 312$ GPa. Note that in Fig. 16 stress discontinuity exits as expected across the fiber–matrix boundary where it passes through the elements.

To demonstrate the applicability of the method to model non-trivial geometry, the fiber or inclusion geometry is modeled as a union of four circles as shown in Fig. 17. A method for defining the step functions for Boolean combination of shapes has been described in past work (Kumar and Lee, 2006). Alternatively, implicit equations can be constructed as signed distance functions for any geometry defined using parametric equations (Osher and Fedkiw, 2002; Burla and Kumar, 2008).

The contour plots for normal and shear stresses for load Cases 1 and 4 are shown in Fig. 17. In this example, the fiber volume ratio of 0.41 was used. The effective properties were computed as: $E_1 = 196$ GPa, $E_2 = E_3 = 132$ GPa, $G_{23} = 44$ GPa, $G_{13} = G_{12} = 51$ GPa, $\nu_{23} = \nu_{32} = 0.269$, $\nu_{13} = \nu_{12} = 0.208$, $\nu_{31} = \nu_{21} = 0.141$. Using the rule of mixtures for the longitudinal modulus shows a good agreement. However, other moduli are not compared with analytical solutions as the geometry used is non-standard.

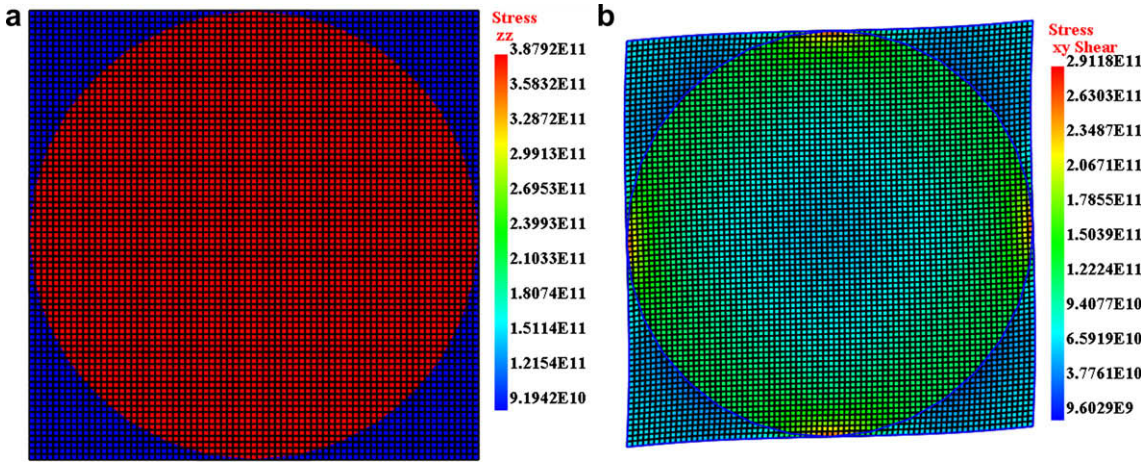

Fig. 16. (a) Plot of σ_{11} normal stress for Case 1 and (b) plot of τ_{23} shear stress for Case 4.

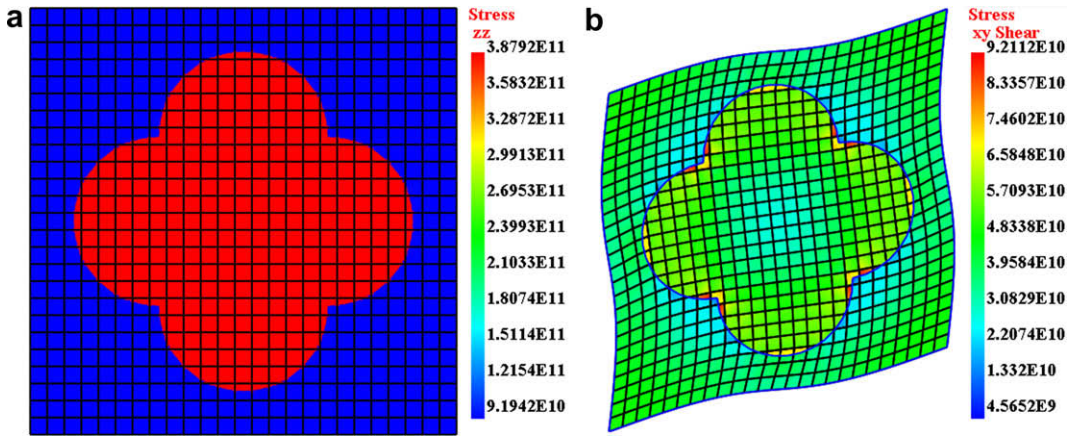

Fig. 17. (a) Plot of σ_{11} normal stress for Case 1 and (b) plot of τ_{23} normal stress for Case 2.

Table 4
State of stress for six different cases in 3D model.

Case	Unit strain	σ_{11}(GPa)	σ_{22}(GPa)	σ_{33}(GPa)	τ_{23}(GPa)	τ_{13}(GPa)	τ_{12}(GPa)
1	$\varepsilon_{11} = 1$	230.57	40.34	40.34	0	0	0
2	$\varepsilon_{22} = 1$	40.35	160.93	46.25	0	0	0
3	$\varepsilon_{33} = 1$	40.35	46.25	160.93	0	0	0
4	$\gamma_{23} = 1$	0	0	0	45.98	0	0
5	$\gamma_{13} = 1$	0	0	0	0	54.37	0
6	$\gamma_{12} = 1$	0	0	0	0	0	54.37

6.3. Example 6.3: computation of effective properties using a three-dimensional model

In this example a three-dimensional model is used for computation of effective properties of the composite modeled in Example 6.2. The results obtained by three-dimensional analysis are compared with the results available in the literature. The periodic boundary conditions shown in Table 1 are used for the analysis. The average values of stresses and strains are tabulated in Table 4, and the effective elastic constants that are determined by the 3D model are tabulated in Table 3. It can be observed that the effective properties determined by 3D model matches very closely with the ones determined by 2D model and with the ones available in the literature. Figs. 18–20 show the stress distribution for various cases.

7. Conclusions

In this paper, a method for imposing material interface conditions is presented by constructing a solution structure based on the implicit equations of the inclusion boundaries. The weak form for linear elasticity was modified using this solution structure such that interface conditions are satisfied exactly for displacements and weakly for the stresses/strains. The primary motivation for the method is the desire to eliminate the need for a mesh that conforms to the interface boundaries and to use implicit equations of curves/surfaces to represent the inclusion instead of using a conforming mesh to approximate it. Generating a uniform structured grid that encloses the geometry is a very straight forward process. One of the advantages of this method is that stiffness matrix integration does not have to be computed for all the elements. Stiffness matrix evaluated for any one element entirely within the inclusion (or matrix) can be used for all other elements within the element (or matrix). It has been shown that the solution structure presented in this work has good convergence properties and is capable of determining the effective elastic constants with very good accuracy. This method holds the potential for determining effective properties of complicated microstructures if the equations of the geometry of the inclusions are imported from computer-aided design software.

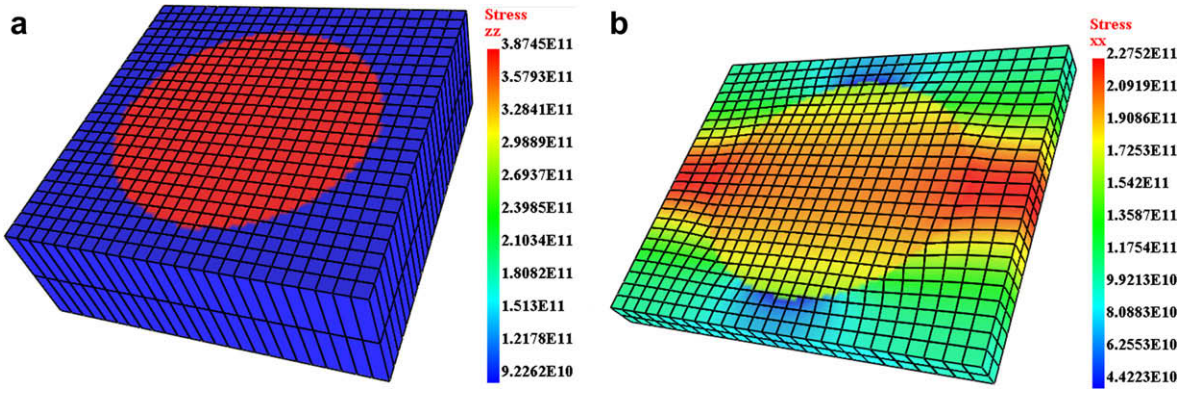

Fig. 18. (a) Plot of σ_{11} normal stress for Case 1 and (b) plot of σ_{22} normal stress for Case 2.

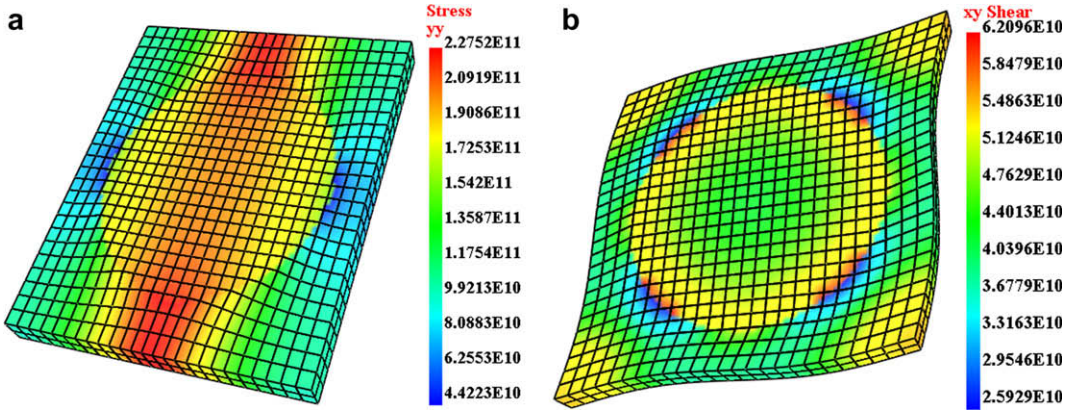

Fig. 19. (a) Plot of σ_{33} normal stress for Case 3 and (b) plot of τ_{23} shear stress for Case 4.

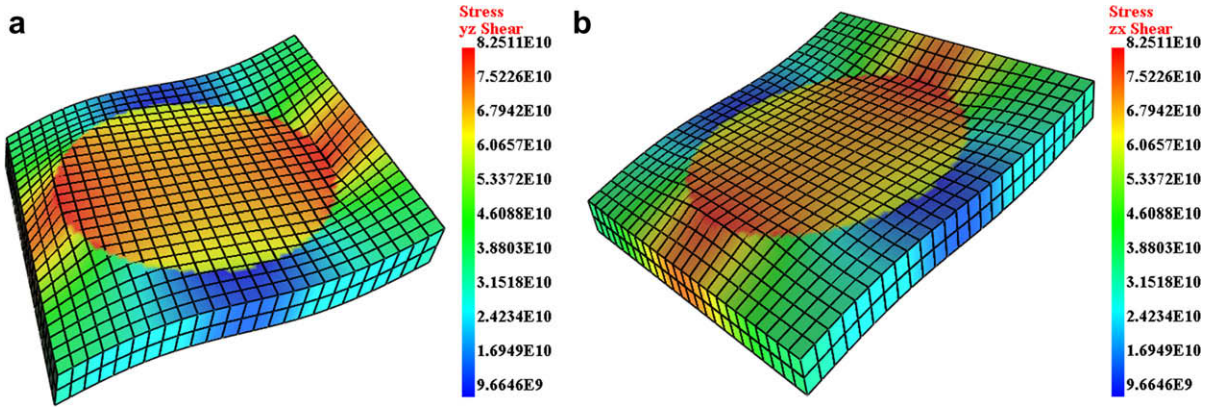

Fig. 20. (a) Plot of τ_{31} shear stress for Case 5 and (b) plot of τ_{12} shear stress for Case 6.

For other types of periodic structures such as hexagonal pattern of fiber packing (Chen and Cheng, 1967), larger RVE that include more fibers will be needed but the method is applicable regardless of the geometry of the microstructure or the inclusions.

Acknowledgements

R.K.B. would like to acknowledge Alumni Fellowship and support from the Department of Mechanical and Aerospace engineering at the University of Florida. The authors would like to acknowledge partial support for this research from AFRL/MN and ARO.

References

Adams, D.F., Crane, D.A., 1984. Finite element micromechanical analysis of a unidirectional composite including longitudinal shear loading. Computers and Structures 6, 1153–1165.
Atluri, S.N., Zhu, T., 1998. New Meshless Local Petrov–Galerkin (MLPG) approach in computational mechanics. Computational Mechanics 22 (2), 117–127.
Belytschko, T., Lu, Y.Y., Gu, L., 1994. Element Free Galerkin methods. International Journal for Numerical Methods in Engineering 37, 229–256.
Belytschko, T., Krongauz, Y., Organ, D., Fleming, M., Krysl, P., 1996. Meshless methods: an overview and recent developments. Computer Methods in Applied Mechanics and Engineering 139 (1–4), 3–47.
Belytschko, T., Parimi, C., Moes, N., Usui, S., Sukumar, N., 2003. Structured extended finite element methods for solids defined by implicit surfaces. International Journal for Numerical Methods in Engineering 56 (4), 609–635.
Burla, R., Kumar, A.V., 2008. Implicit boundary method for analysis using uniform B-spline basis and structured grid. International Journal for Numerical Methods in Engineering 76 (13), 1993–2028.
Cai, Y.C., Zhu, H.H., 2004. Direct imposition of essential boundary conditions and treatment of material discontinuities in the EFG method. Computational Mechanics 34 (4), 330–338.
Chamis, C.C., 1984. Simplified composite micromechanics equations for hygral, thermal and mechanical properties. SAMPE Quarterly, 14–23.
Chen, C.H., Cheng, S., 1967. Mechanical properties of fiber reinforced composites. Journal of Composite Materials, 30–41.
Cook, R.D., Malkus, D.S., Plesha, M.E., Witt, R.J., 2003. Concepts and Applications of Finite Element Analysis. John Wiley and Sons Inc., New York.
Cordes, L.W., Moran, B., 1996. Treatment of material discontinuity in the element-free Galerkin method. Computer Methods in Applied Mechanics and Engineering 139 (1–4), 75–89.
Dang, T.D., Sankar, B.V., 2007. Meshless local Petrov–Galerkin formulation for problems in composite micromechanics. AIAA Journal 45 (4), 912–921.
De, S., Bathe, K.J., 2000. Method of finite spheres. Computational Mechanics 25 (4), 329–345.
Qu, J., Cherkaoui, M., 2006. Fundamentals of Micromechanics of Solids. John Wiley and Sons Inc., New Jersey.
Höllig, K., 2003. Finite Element Methods with B-Splines. SIAM, Philadelphia.
Kantorovich, L.V., Krylov, V.I., 1958. Approximate Methods of Higher Analysis. Interscience, New York.
Kim, H.J., Swan, C.C., 2003. Algorithms for automated meshing and unit cell analysis of periodic composites with hierarchical tri-quadratic tetrahedral elements. International Journal for Numerical Methods in Engineering 58 (11), 1683–1711.
Krongauz, Y., Belytschko, T., 1998. EFG approximation with discontinuous derivatives. International Journal for Numerical Methods in Engineering 41 (7), 1215–1233.
Kumar, A.V., Padmanabhan, S., Burla, R., 2007. Implicit boundary method for finite element analysis using non-conforming mesh or grid. International Journal for Numerical Methods in Engineering 74 (9), 1421–1447.
Kumar, A.V., Lee, J., 2006. Step function representation of solid models and application to mesh free engineering analysis. Journal of Mechanical Design, ASME 128, 1–11.
Li, S., Lim, S.H., 2005. Variational principles for generalized plane strain problems and their applications. Applied Science and Manufacturing 36 (3), 353–365.
Marrey, R.V., Sankar, B.V., 1997. A micromechanical model for textile composite plates. Journal of Composite Materials 31 (12), 1187–1213.
Oden, J.T., Duarte, C.A.M., Zienkiewicz, O.C., 1998. New cloud-based hp finite element method. Computer Methods in Applied Mechanics and Engineering 153 (1–2), 117–126.

Osher, S.J., Fedkiw, R.P., 2002. Level Set Methods and Dynamic Implicit Surfaces. Springer Verlag, Philadelphia.
Shapiro, V., Tsukanov, I., 1999. Meshfree simulation of deforming domains. Computer-Aided Design 31, 459–471.
Sukumar, N., Moran, B., Yu, S.A., Belikov, V.V., 2001. Natural neighbor Galerkin methods. International Journal for Numerical Methods in Engineering 50, 1–27.
Sun, C.T., Chen, J.L., 1990. A micromechanical model for plastic behavior of fibrous composites. Composites Science and Technology 40, 115–129.
Sun, C.T., Vaidya, R.S., 1996. Prediction of composite properties from a representative volume element. Composites Science and Technology 56 (2), 171–179.
Taliercio, A., 2005. Generalized plane strain finite element model for the analysis of elastoplastic composites. International Journal of Solids and Structures 42 (8), 2361–2379.
Whitney, J.M., Riley, M.B., 1966. Elastic properties of fiber reinforced composite materials. AIAA Journal 4, 1537–1542.
Xia, Z., Zhang, Y., Ellyin, F., 2003. A unified periodical boundary conditions for representative volume elements of composites and applications. International Journal of Solids and Structures 40 (8), 1907–1921.
Zhu, H., Sankar, B.V., Marrey, R.V., 1998. Evaluation of failure criteria for fiber composites using finite element micromechanics. Journal of Composite Materials 32 (8), 766–782.